Does a fast mixer really exist?

Weijiu Liu*
Department of Mathematics, University of Central Arkansas, 201 Donaghey Avenue, Conway, Arkansas 72034, USA
(Received 3 March 2005; revised manuscript received 2 May 2005; published 26 July 2005)

In this paper, we are concerned about the limit behavior of the decay rate of variance of a passive and diffusive scalar in a flow field as the diffusivity of the scalar goes to zero. Motivated by the concept of the fast dynamo in the dynamo theory, we term a flow as *fast mixer* if the decay rate remains away from zero as the diffusivity goes to zero. We first repeat numerical simulations with flow maps and velocity fields used in the existing literature, including the lattice map, the 1D baker's map, and the sinusoidal shear flow. Our simulations shows that, in all cases, the decay rate tends to zero as the diffusivity goes to zero. For the closed flows in a bounded domain, we then theoretically proved this result under certain plausible conditions on the flows. For the open flows in the whole space, we show that the effective diffusivity matrix tends to zero in the limit without the conditions for the closed flow. In conclusion, although a fast mixer might exist, it could be very difficult to find one.

DOI: 10.1103/PhysRevE.72.016312 PACS number(s): 47.27.Te

I. INTRODUCTION

In the theory of fluid mixing, it is of practical interest to understand the limit behavior of the decay rate of variance of a passive and diffusive scalar in a flow field as the diffusivity of the scalar goes to zero. The passive and diffusive scalar is some physical entity, such as chemical pollutants dispersing in the environment or dyes used in visualizing flow patterns, which is immersed in the fluid flow and does not significantly influence the fluid motion. The scalar undergoes two processes, molecular diffusion and passive advection by the flow.

The evolution of the scalar can be mathematically modeled by the advection-diffusion equation

$$c_t + \nabla c \cdot \mathbf{v} = \kappa \Delta c \tag{1}$$

in the absence of a source, where $\mathbf{v}(\mathbf{x},t)$ denotes a velocity field on a bounded domain S in $\mathbb{R}^n$, $c(\mathbf{x},t)$ the concentration of the scalar, and $\kappa>0$ (cm^2/s) the molecular diffusivity of the scalar. Throughout the paper, we assume that $\mathbf{v}$ is incompressible ($\nabla\cdot\mathbf{v}=0$), and satisfies periodic, no-flow, or no-slip boundary conditions on the boundary ∂S.

In the above model, the advection process and diffusion process concur. However, for the need of investigation, these two processes are sometimes separated into two phases and described mathematically by two equations. For instance, when Pierrehumbert [1] explored the mixing induced by the map

$$x_{n+1} = x_n + a \sin[2\pi(y_n + \varphi_n)] \pmod 1, \tag{2}$$

$$y_{n+1} = y_n + \cos[2\pi(x_{n+1} + \psi_n)] \pmod 1, \tag{3}$$

where φ_n and ψ_n are random variables uniformly distributed over $[0,1]$ and a is a constant, the mixing process was numerically modeled in two phases. First, the map was used to stir a scalar and rearrange its concentration $c(x,y,n)$ by

$$c(x_{n+1},y_{n+1},n+1) = c(x_n,y_n,n), \tag{4}$$

where (x_n,y_n) varies across all grid points on a regular grid at $(n+1)$th iteration. Then the diffusion process was realized by

$$c_{ij}^{n+2} = (1-\kappa)c_{ij}^{n+1} + \frac{\kappa}{4}(c_{i+1,j}^{n+1} + c_{i-1,j}^{n+1} + c_{i,j+1}^{n+1} + c_{i,j-1}^{n+1}), \tag{5}$$

where $c_{ij}^n = c(x_i,y_j,n)$ denotes the concentration on the regular grid at the nth iteration.

Another similar example is the mixing induced by the one-dimensional baker's map studied in [2]

$$x_n = \begin{cases} x_{n+1}/\alpha & \text{if } 0 \leqslant x_{n+1} < \alpha, \\ (x_{n+1}-\alpha)/(1-\alpha) & \text{if } \alpha \leqslant x_{n+1} \leqslant 1. \end{cases} \tag{6}$$

For this mixing process, the scalar was stirred by the map at time $t=nT$ ($T>0$) through

$$c_1(x_{n+1},nT) = \begin{cases} c(x_{n+1}/\alpha,nT) & \text{if } 0 \leqslant x_{n+1} < \alpha, \\ c[(x_{n+1}-\alpha)/(1-\alpha),nT] & \text{if } \alpha \leqslant x_{n+1} \leqslant 1. \end{cases} \tag{7}$$

Between the times $t=nT$ and $(n+1)T$, the diffusive process is governed by the one-dimensional diffusion equation

$$\frac{\partial c}{\partial t} = \kappa \frac{\partial^2 c}{\partial x^2},$$

$$c(x,nT) = c_1(x,nT). \tag{8}$$

The model (1) should be different from the model (4) and (5) or (7) and (8). Indeed, the latter is not a discretized version of the former and cannot be written in the form of (1). Since the advection and diffusion processes should concur in practical problems, (1) could be a better model.

Motivated by the concept of the fast dynamo in the dynamo theory (see, e.g., [3]), we term a flow as *fast mixer* if the decay rate remains away from zero as the diffusivity goes to zero. It has become a controversial problem whether or not there exists such a fast mixer.

*Electronic address: liuweijiu@hotmail.com

 ©2005 The American Physical Society

Efforts have been made to show the existence of a fast mixer. Exploring the mixing induced by the lattice map (2) and (3), Pierrehumbert [1] observed that the variance decays corresponding to two small diffusivites were very close and then conjectured that the lattice map could be a fast mixer. With the model (7) and (8), Fereday *et al.* [3] approximately computed the decay rates and observed that the value of the decay rate is essentially independent of κ in the small κ limit. Antonsen *et al.* [4] investigated a two-dimensional chaotic cosine flow and numerically showed that the flow is a fast mixer.

On the other hand, there is also evidence showing that the limit decay rate is zero. Generally speaking, finding such evidence is easier than finding the evidence for the fast mixer because large classes of flows are not fast mixers. Observing logarithmic or power-law dependence on the diffusivity for some three-dimensional steady flows, Toussaint *et al.* [5] pointed out that such flows are in the class of zero limit. Pikovsky and Popovych [6] showed that the largest eigenvalue λ of the Frobenius-Perron operator induced by a cosine flow map approaches 1 and then the decay rate $\ln\lambda$ goes to zero as the diffusivity tends to zero. Giona *et al.* [7,8] proved that the eigenvalue (which is the decay rate) of the advection-diffusion operator with a steady sine flow converges to zero at the rate κ^{α} ($\alpha>0$). For open flows in an unbounded domain, Fannjiang and Papanicolaou [9] showed that the effective diffusivity is proportional to the square root of the diffusivity.

In this paper, we first repeat numerical simulations with flow maps and velocity fields used in the existing literature in Sec. III, including the lattice map (2) and (3) (see [1]), the 1D baker's map (6) (see [2,10]), and the sinusoidal shear flow (see, e.g., [4,11]). Our simulations show that, in all cases, the decay rate tends to zero as $\kappa\to 0$. Then in Sec. IV, this result is theoretically proved under certain plausible conditions on the closed flows in a bounded domain. For the open flows in the whole space, we show that the effective diffusivity matrix tends to zero in the limit without the conditions for the closed flow. In conclusion, although a fast mixer might exist, it could be very difficult to find one.

II. DEFINITION AND PROPERTIES OF DECAY RATE

Consider now a diffusive scalar $c(\mathbf{x},t)$ on a bounded domain S of two- or three-dimensional spaces. For simplicity, we assume the zero mean concentration

$$\langle c\rangle = \int_S c(\mathbf{x},t)dA = 0.$$

Mathematically we assume that the evolution of the scalar is governed by either the original advection-diffusion equation (1) or the simplified models such as the lattice model (4) and (5) and the 1D bakers model (6)–(8).

In general, the concentration $c(\mathbf{x},t)$ depends on the diffusivity κ and initial concentrations $c^0(\mathbf{x})$. In what follows, when we address the problem of its dependence on κ and c^0, we will explicitly write it as $c(\mathbf{x},t;\kappa,c^0)$ or $c_\kappa(\mathbf{x},t;c^0)$. Otherwise, we always suppress the κ or c^0 for brevity.

To motivate us to define the decay rate of variance of the scalar, we first look at the special case of the time-periodic velocity $\mathbf{v}(\mathbf{x},t)$. In this case, we showed in [12] that the solution c of (1) with an initial concentration $c^0(\mathbf{x})$ can be expanded in terms of eigenmodes as follows:

$$c(\mathbf{x},t;\kappa,c^0) = \sum_{k=1}^{N} e^{\lambda_k t} e_k(\mathbf{x},t;\kappa,c^0) + R(\mathbf{x},t;\kappa,c^0), \qquad (9)$$

where $\lambda_k=\lambda_k(\kappa,c^0)$ are Floquet exponents with the corresponding eigenmodes $e_k(\mathbf{x},t;\kappa,c^0)$ and the remainder $R(\mathbf{x},t;\kappa,c^0)$ is small. By eigenmodes here we mean that $e_k(\mathbf{x},t;\kappa,c^0)$ has the following form:

$$e_k(\mathbf{x},t;\kappa,c^0) = c_0(\mathbf{x},t;\kappa,c^0) + tc_1(\mathbf{x},t;\kappa,c^0) + \cdots + t^{l(k)}c_{l(k)}(\mathbf{x},t;\kappa,c^0)$$

and $e^{\lambda_k t}e_k(\mathbf{x},t;\kappa,c^0)$ is a solution of (1), where $l(k)\geqslant 0$ is a non-negative integer, and $c_i(\mathbf{x},t;\kappa,c^0)$ are continuous time-periodic functions. Let λ_1 be the Floquet exponent with the largest real part. It then follows from (9) that

$$c(\mathbf{x},t;\kappa,c^0) = e^{\lambda_1 t}t^n F(\mathbf{x},t;\kappa,c^0),$$

where n is a non-negative integer and the L^2 norm of F is bounded over $t\in[1,\infty)$. Taking the L^2 norm of the above, we obtain that

$$\begin{aligned}\mathrm{Re}[\lambda_1(\kappa,c^0)] &= \lim_{t\to\infty}\frac{1}{t}\ln\|c(t;\kappa,c^0)\|_2 - \lim_{t\to\infty}\frac{1}{t}\ln t^n \\ &\quad - \lim_{t\to\infty}\frac{1}{t}\ln\|F(t;\kappa,c^0)\|_2 \\ &= \lim_{t\to\infty}\frac{1}{t}\ln\|c(t;\kappa,c^0)\|_2,\end{aligned}$$

where

$$\|c(t;\kappa,c^0)\|_2^2 = \int_S |c(\mathbf{x},t;\kappa,c^0)|^2 dA.$$

Thus the decay rate corresponding to the initial concentration c^0 in this case, denoted by $\gamma(\kappa,c^0)$, is equal to

$$\gamma(\kappa,c^0) = -\mathrm{Re}(\lambda_1) = -\lim_{t\to\infty}\frac{1}{t}\ln\|c(t;\kappa,c^0)\|_2.$$

For general velocities, the above limit may not exist. Thus we define the decay rate corresponding to the initial concentration c^0 in general cases by

$$\gamma(\kappa,c^0) = -\limsup_{t\to\infty}\frac{1}{t-t_0}\ln\frac{\|c(t;\kappa,c^0)\|_2}{\|c^0\|_2}. \qquad (10)$$

Here we have divided $\|c(t;\kappa,c^0)\|_2$ by $\|c^0\|_2$ to normalize the c. The decay rate of the scalar field is defined by

$$\Gamma(\kappa) = \inf_{c^0}\gamma(\kappa,c^0). \qquad (11)$$

In what follows, when we address the problem of dependence of γ on κ or c^0, we will explicitly write γ as a function

$\gamma(\kappa, c^0)$ of κ and c^0. Otherwise, we always suppress the κ or c^0 for brevity.

In computation, the rate can be calculated by the following approximate formula:

$$\gamma(t) = -\frac{1}{t-t_0} \ln \frac{\|c(t)\|_2}{\|c^0\|_2}, \quad t \text{ large}. \tag{12}$$

To get an accurate value of γ, we should take t to be so large that $\gamma(t)$ has reached a steady state. But the time t should not be too large since $\|c(t)\|_2$ may become constant after the scalar field has been transited to the steady state at some large time T and then

$$-\frac{1}{t-t_0} \ln \frac{\|c(t)\|_2}{\|c^0\|_2}$$

may go to zero if $t \to \infty$. Therefore, we should carefully choose an appropriate t in computation.

The following property could explain why the number γ defined in (10) is called the decay rate.

Proposition 2.1: *For any* $\varepsilon > 0$, *there exists a positive constant* $M(\varepsilon)$ *such that*

$$\|c(t)\|_2 \leqslant M(\varepsilon)\|c^0\|_2 \exp[(\varepsilon - \gamma)(t-t_0)] \quad \text{for all } t \geqslant t_0. \tag{13}$$

Proof: By the definition (10), there exists $T = T(\varepsilon)$ such that

$$\sup_{t \geqslant T} \frac{1}{t-t_0} \ln \frac{\|c(t)\|_2}{\|c^0\|_2} \leqslant -\gamma + \varepsilon,$$

which implies that

$$\|c(t)\|_2 \leqslant \|c^0\|_2 \exp[(\varepsilon - \gamma)(t-t_0)] \quad \text{for all } t \geqslant T.$$

We define

$$B(\varepsilon) = \sup_{t_0 < t \leqslant T} \frac{1}{t-t_0} \ln \frac{\|c(t)\|_2}{\|c^0\|_2}.$$

Although the above expression is singular at $t = t_0$, $B(\varepsilon)$ is finite and negative since $\|c(t)\|_2 \leqslant \|c^0\|_2$ due to the diffusion. We then deduce that

$$\begin{aligned}\|c(t)\|_2 &\leqslant \|c^0\|_2 \exp(B(\varepsilon)(t-t_0)) \\ &= \exp\{[B(\varepsilon) - \varepsilon + \gamma](t-t_0)\}\|c^0\|_2 \exp\{[\varepsilon - \gamma)(t-t_0]\} \\ &\quad \text{for all } t_0 \leqslant t \leqslant T.\end{aligned}$$

It therefore follows that (13) holds with

$$M(\varepsilon) = \max\{1, \sup_{t_0 \leqslant t \leqslant T(\varepsilon)} \exp([B(\varepsilon) - \varepsilon + \gamma](t-t_0))\}. \tag{14}$$

Generally speaking, the constant $M(\varepsilon)$ may go to infinity as $\varepsilon \to 0$. For instance, let us consider the simple function $f(t) = e^{-t+\sqrt{t}}$. Evidently, its decay rate γ is equal to 1. Since

$$f(t) = e^{\sqrt{t}-\varepsilon t} e^{(\varepsilon - 1)t},$$

we have

$$M(\varepsilon) = \sup_{0 \leqslant t \leqslant \infty} e^{\sqrt{t}-\varepsilon t} = e^{1/(4\varepsilon)},$$

which converges to infinity as $\varepsilon \to 0$. However, there are many functions such that the constant $M(\varepsilon)$ is uniformly bounded $\varepsilon \to 0$, for example, $f(t) = e^{-t+1}$.

The uniform boundedness of $M(\varepsilon)$ plays an important role in the fast mixer problem. Since the number ε in (13) is arbitrary, we can replace it by the diffusivity κ. If $M(\kappa)$ is uniformly bounded as $\kappa \to 0$, we will be able to prove that the decay rate $\gamma(\kappa)$ converges to zero as $\kappa \to 0$ in Sec. IV. Hence, the study of such uniform boundedness becomes crucial.

For the pure diffusion processes without advection by a flow, it is well known that the decay rate Γ is equal to the smallest eigenvalue of the Laplacian $-\kappa\Delta$ and $M(\kappa) = 1$ is independent of κ. If the advection is present, numerical simulations in Sec. IV show that there may be many flows and maps like 1D baker's maps such that $M(\kappa)$ is uniformly bounded (see Figs. 7 and 8 below). However, their theoretical proofs are open and could be difficult.

The following property shows that the decay rate γ is the largest number λ such that there exists a positive constant M such that

$$\|c(t)\|_2 \leqslant M\|c^0\|_2 \exp[-\lambda(t-t_0)] \text{ for all } t \geqslant t_0$$

holds.

Proposition 2.2: For the decay rate defined in (10) we have

$$\gamma = \sup\left\{\lambda \Big| \sup_{t \geqslant t_0} e^{\lambda(t-t_0)} \frac{\|c(t)\|_2}{\|c^0\|_2} < \infty\right\}. \tag{15}$$

Proof: Denote

$$\Lambda = \left\{\lambda \Big| \sup_{t \geqslant t_0} e^{\lambda(t-t_0)} \frac{\|c(t)\|_2}{\|c^0\|_2} < \infty\right\}.$$

By (13), we have $\gamma - \varepsilon \in \Lambda$ for any $\varepsilon > 0$ and then $\gamma \leqslant \sup \Lambda$. On the other hand, for any $\varepsilon > 0$, there exists $T_0 = T_0(\varepsilon)$ such that

$$\sup_{t \geqslant T} \frac{1}{t-t_0} \ln \frac{\|c(t)\|_2}{\|c^0\|_2} > -\gamma - \varepsilon, \quad \text{for all } T \geqslant T_0,$$

which implies that there exists $t_n \to \infty$ such that

$$\frac{1}{t_n - t_0} \ln \frac{\|c(t_n)\|_2}{\|c^0\|_2} > -\gamma - \varepsilon,$$

and then

$$e^{(\gamma+2\varepsilon)(t_n-t_0)} \frac{\|c(t)\|_2}{\|c^0\|_2} > e^{\varepsilon(t_n-t_0)}.$$

This shows that $\gamma + 2\varepsilon \notin \Lambda$ and then $\gamma \geqslant \sup \Lambda$. Therefore (15) holds.

In the above discussions, the scalar does not need to evolve according to the advection-diffusion equation (1). However, if it follows the equation, then we can show that its

decay rate is greater than the smallest eigenvalue of the Laplacian $-\kappa\Delta$. For this, we complete the equation with initial and boundary conditions as follows:

$$c_t + \nabla c \cdot \mathbf{v} = \kappa \Delta c,$$

$$c(\mathbf{x}, t_0) = c^0(\mathbf{x}),$$

$$\left.\frac{\partial c}{\partial n}\right|_{\partial S} = 0 \tag{16}$$

with $c^0(\mathbf{x})$ denoting the initial concentration at $t=t_0$, and with $\partial c/\partial n|_{\partial S}$ referring to the normal derivative of c along the boundary ∂S. In this paper, we fix the above Neumann boundary condition for concreteness, but our results in this paper are equally valid for Dirichlet or spatially periodic boundary conditions.

Proposition 2.3: If the diffusive scalar $c(\mathbf{x},t)$ evolves according to the problem (16), then the decay rate satisfies $\Gamma \geqslant \kappa\mu_1$, where the constant μ_1 is the smallest eigenvalue of the Laplacian $-\Delta$ with the boundary condition in (16).

Proof: Multiplying (16) by c and integrating over the domain S gives the well-known result

$$\frac{1}{2}\frac{d}{dt}\|c\|_2^2 = -\kappa\|\nabla c\|_2^2. \tag{17}$$

Applying the Poincaré inequality

$$\mu_1\|c\|^2 \leqslant \|\nabla c\|^2, \tag{18}$$

we obtain the estimate

$$\|c(\mathbf{x},t)\|_2^2 \leqslant \|c_0\|_2^2 e^{-2\kappa\mu_1(t-t_0)}, \tag{19}$$

where the constant μ_1 is the smallest eigenvalue of the Laplacian $-\Delta$. It therefore follows that

$$\ln\frac{\|c(t)\|_2}{\|c_0\|_2} \leqslant -\kappa\mu_1(t-t_0),$$

which implies that $\gamma(c^0) \geqslant \kappa\mu_1$ for all c^0 and then $\Gamma \geqslant \kappa\mu_1$.

The numerical simulations in the next section will show that the decay rate $\gamma(c^0)$ for some c^0 is indeed much greater than the smallest eigenvalue of the Laplacian $-\kappa\Delta$ if the scalar field is well stirred by a flow, that is, mixing is enhanced. Although the decay rate Γ is equal to $\inf_{c^0}\{\gamma(c^0)\}$, it is quite possible that Γ is also greater than the smallest eigenvalue.

III. NUMERICAL EXAMPLES

In this section, we repeat numerical simulations with flow maps and velocity fields used in the existing literature, including the lattice map (2) and (3) (see [1]), the 1D baker's map (6) (see [2,10]), and the sinusoidal shear flow (see, e.g., [4,11]). Our simulations show that, in all cases, the decay rate $\gamma(\kappa, c^0)$ for some c^0 tends to zero as $\kappa \to 0$, and so does the decay rate $\Gamma(\kappa)$ since it is equal to $\inf_{c^0}\{\gamma(\kappa, c^0)\}$. We start with the lattice map.

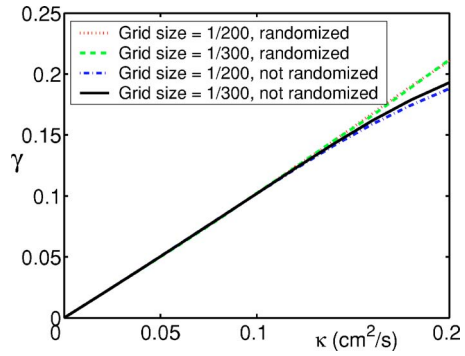

FIG. 1. (Color online) Decay rate of variance for the mixing induced by the map (2) and (3) with $a=4$. The solid, dotted-dashed, dashed, and dotted curves stand for the simulated rates in the cases of the grid sizes 1/300, 1/200 without random disturbances, 1/300, and 1/200 with random disturbances, respectively. The decay rates are simulated for 21 different diffusivities $\kappa(\mathrm{cm}^2/\mathrm{s})$ ranging from 0 to 0.2 with the even spacing of 1/20 $(\mathrm{cm}^2/\mathrm{s})$.

A. Pierrehumbert's sine-cosine map

The flow map (2) and (3) was first proposed by Pierrehumbert in [1] and used in [4,13]. In our simulation here, we use the same numerical scheme (4) and (5).

In order to see whether or not our simulation results change when the space grid size is varied, we consider two different grids of the unit square $[0,1]\times[0,1]$. One grid has 200×200 grid points and the other has 300×300 ones. On these grids, the concentration c is first rearranged by the map (2) and (3) through (4) and then undergoes the diffusion process through (5).

To see the effect of small random disturbances on the decay rate, we consider both randomized and unrandomized maps.

In our computations, we take the same value $a=4$ and the same initial condition $c^0(x,y)=\cos(2\pi x)\cos(2\pi y)$ as in [1]. We simulate the decay rates for 21 different diffusivities κ $(\mathrm{cm}^2/\mathrm{s})$ ranging from 0 to 0.2 with the even spacing of 1/20 (cm/s). For each diffusivity κ, 40 iterations are run. The approximate decay rate $\gamma(\kappa)$ is computed by the formula (12).

In Fig. 1, the solid, dotted-dashed, dashed, and dotted curves stand for the simulated rates in the cases of the grid sizes 1/300, 1/200 without random disturbances, 1/300, and 1/200 with random disturbances, respectively. This figure clearly shows that $\gamma(\kappa)\to 0$ as $\kappa\to 0$ in all cases. From the figure, we can also see that there are no big differences between the randomized and unrandomized maps and no big changes when the grid size is varied, especially for the small diffusivity.

B. 1D baker's map

The 1D baker's map (see [2,10]) is defined by (6). In our simulation here we use the same numerical scheme (6)–(8). The diffusion equation (8) is considered on the unit interval [0,1] with periodic boundary conditions. Then the concentration c can be expressed by the following Fourier series:

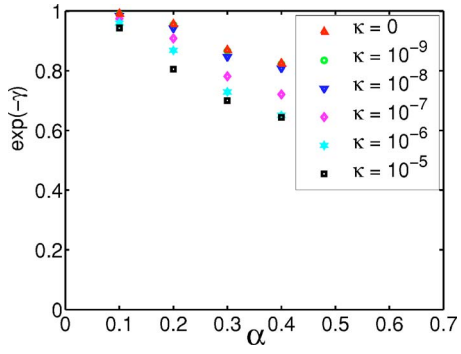

FIG. 2. (Color online) Decay factor $|\mu|=e^{-\gamma}$ of variance of the mixing induced by the 1D baker's map (6) as a function of α for six different small diffusivities $\kappa=0,10^{-9},10^{-8},10^{-7},10^{-6},10^{-5}(\mathrm{cm}^2/\mathrm{s})$. These factors are computed with the use of Fourier series (20).

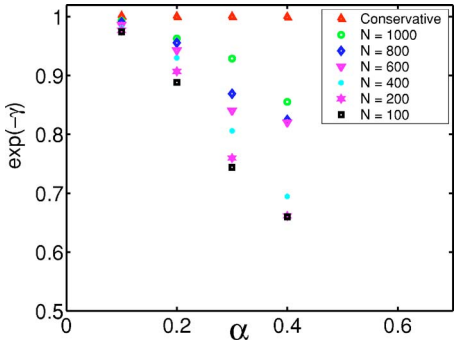

FIG. 3. (Color online) Decay factor $|\mu|=e^{-\gamma}$ of variance of the mixing induced by the 1D baker's map (6) as a function of α for different truncations $N=100,200,400,600,800,1000$, with $\kappa=0$ $(\mathrm{cm}^2/\mathrm{s})$. "Conservative" indicates that the factor is computed without the use of Fourier series (20) while it is used in other cases.

$$c(\mathbf{x},t)=a_0+\sum_{n=1}^{\infty}e^{-4\kappa n^2\pi^2 t}[a_n\cos(2n\pi x)+b_n\sin(2n\pi x)]. \tag{20}$$

According to the numerical scheme (6)–(8), the scalar field is advected by the map at every interval of time T, and then, between the advection of the map, the scalar field evolves according to the above series.

We compute the decay rates for four different $\alpha=0.1,0.2,0.3,0.4$ and six different small diffusivities $\kappa=0,10^{-9},10^{-8},10^{-7},10^{-6},10^{-5}$ $(\mathrm{cm}^2/\mathrm{s})$ as shown in Fig. 2, especially the zero diffusivity being included for the reason we will explain below. In our computations, we take the period $T=1$ and the initial condition $c^0(x)=\sin(2\pi x)$. The series is truncated at $N=800$, the interval $[0,1]$ is divided into 3000 subintervals for numerical integrations of the Fourier coefficients, and the approximate decay rate $\gamma(\kappa)$ is computed by the formula (12).

To compare our result with the one in [2], we notice that, instead of computing γ, the eigenvalue μ of a truncated transfer matrix with the largest modulus was calculated in [2] and the relation between γ and μ is $\gamma=-\ln|\mu|$. Therefore, we plot $|\mu|=e^{-\gamma}$, instead of γ, in Fig. 2. With this in mind, it can been seen from the figure that our result is very close to the one obtained in [2] and the decay rate γ converges to a positive number ($|\mu|=e^{-\gamma}$ converges to a positive number less than 1) in the cases of $\alpha=0.2,0.3,0.4$, respectively.

However, this does not prove that the 1D baker's map is a fast mixer. To see this, we have particularly computed the decay rate in the case of zero diffusivity by using the same procedure for the nonzero diffusivities, that is, before the concentration $c(\mathbf{x},i)$ is advected by the map at the time $t=i+1$, c is expanded as the Fourier series

$$\begin{aligned}c(\mathbf{x},i+1)&=a_0+\sum_{n=1}^{N}e^{-4*0*n^2\pi^2(i+1)}[a_n\cos(2n\pi x)+b_n\sin(2n\pi x)]\\&=a_0+\sum_{n=1}^{N}[a_n\cos(2n\pi x)+b_n\sin(2n\pi x)],\end{aligned} \tag{21}$$

where a_0, a_n, and b_n are the Fourier coefficients of $c(\mathbf{x},i)$. Following this procedure, we obtain a positive rate ($\gamma>0$ while $|\mu|=e^{-\gamma}<1$) for the zero diffusivity as shown in Fig. 2. However, this positive rate is certainly wrong because the rate in this case should be equal to zero. In fact, if the diffusivity is zero, then the scalar field should not undergo the diffusion process. So $c(\mathbf{x},i)$ is advected immediately by the map at the time $t=i+1$ without expanding it as in (21). If we do so, we do obtain the zero rates for $\alpha=0.1,0.2,0.3,0.4$, as indicated by "Conservative" in Fig. 3, since the baker's map is mass-preserved. In this figure, $\kappa=0$ and "Conservative" indicates that the factor is computed without the use of Fourier series (20) while it is used in other cases. Therefore, this positive rate should be the result of the truncation errors and numerical integration errors in the Fourier expansion in (21). To see this, we truncate the series at $N=100,200,400,600,800,1000$. Figure 3 shows that the rate γ is decreasing ($e^{-\gamma}$ increasing) as N increases.

Furthermore, Fig. 2 suggests that $\gamma(\kappa)$ may be a continuous function of κ since $\gamma(10^{-9})$ is almost equal to $\gamma(0)$. If this is really true, then we have $\gamma(\kappa)\to\gamma(0)=0$ as $\kappa\to 0$.

To further confirm that the limit of rate should be zero, we discretize the diffusion equation (8) by central difference in space and the forward difference in time. It is well known that for small diffusivities this scheme is stable and the solution of the difference equation converges to the exact solution of the diffusion equation (see, e.g., [14]). In the computation, the time step is 0.001 and the space grid size is 0.0001. We consider eleven different small diffusivities $\kappa=0,10^{-14},10^{-13},10^{-12},10^{-11},10^{-10},10^{-9},10^{-8},10^{-7},10^{-6},10^{-5}$ $(\mathrm{cm}^2/\mathrm{s})$. Figure 4 shows that $\gamma(\kappa)\to 0$ as $\kappa\to 0$.

To verify the theoretical result of Proposition 2.3 [strictly speaking, it cannot be applied to this case because it was proved for only model (16)] and see that the 1D baker's map greatly enhances mixing, we simulate the decay rates for $\alpha=0.1,0.2,0.3,0.4$ and plot them as functions of κ in Fig. 5. It is well known that the largest eigenvalue of the Laplacian operator $\partial^2/\partial x^2$ with periodic boundary conditions on $[0,1]$ is $-\pi^2$. We plot the function $\gamma=\pi^2\kappa$ in Fig. 5 to compare with the simulated decay rates. The figure clearly shows that the decay rate of the stirred scalar is much greater than $\kappa\pi^2$. As

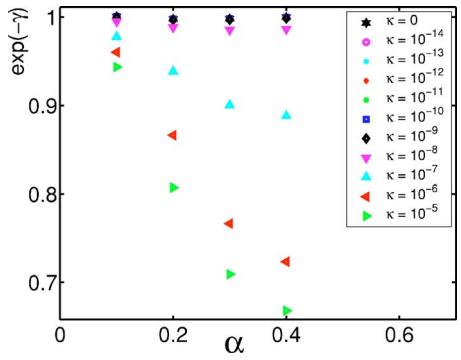

FIG. 4. (Color online) Decay factor $|\mu|=e^{-\gamma}$ of variance of the mixing induced by the 1D baker's map (6) as a function of α for eleven different small diffusivities $\kappa=0,10^{-14},10^{-13},10^{-12},10^{-11},10^{-10},10^{-9},10^{-8},10^{-7},10^{-6},10^{-5}$ (cm^2/s). These factors are computed by using the finite difference method.

we discussed in [12], γ actually is the eigenvalue of the Laplacian operator plus the map. Therefore, the map greatly shifts the original eigenvalue $-\kappa\pi^2$ to the left $-\gamma$.

C. Sinusoidal shear flow

The sinusoidal shear flow (see, e.g., [4,11]) is defined by

$$v_1(x,y,n+t)=\begin{cases} U\sin[2\pi(y+\phi_n)], & 0<t<0.5,\\ 0, & 0.5<t<1,\end{cases} \tag{22}$$

$$v_2(x,y,n+t)=\begin{cases} 0, & 0<t<0.5,\\ U\sin[2\pi(x+\psi_n)], & 0.5<t<1,\end{cases} \tag{23}$$

where ϕ_n and ψ_n are random variable uniformly distributed over $[0,1]$ and U is a constant. In our simulation here the velocity is not randomized, that is, $\phi_n=\psi_n=0$, $U=1$, and the initial condition is $c^0(x,y)=\sin(2\pi x)$.

The advection-diffusion equation (16) with periodic boundary conditions on the unit square $[0,1]\times[0,1]$ is

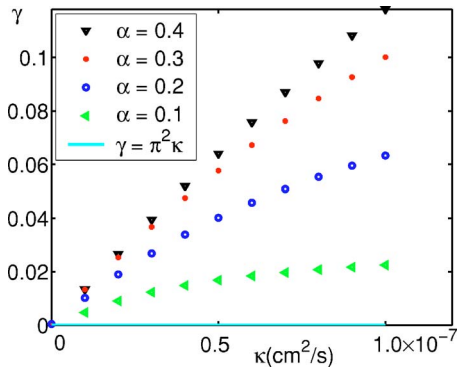

FIG. 5. (Color online) Decay rates γ of variance of the mixing induced by the 1D baker's map (6) as a function of κ (cm^2/s) for $\alpha=0.1,0.2,0.3,0.4$. These rates are computed by using the finite difference method.

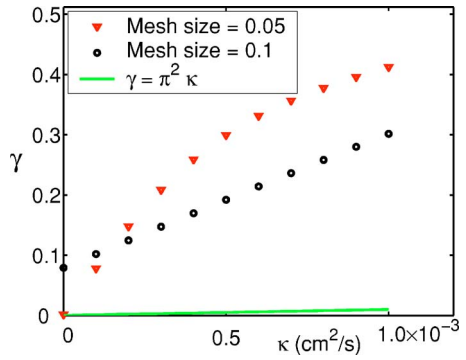

FIG. 6. (Color online) Decay rates of variance for the mixing induced by the sine shear flow (22) and (23) with $U=1$.

solved by using the finite element method codes developed in [15] (with some modifications for this particular problem). The mesh of four-node isoparametric quadrilateral elements is used and the codes are run twice with different mesh sizes 0.1 and 0.05.

In the case of the mesh size 0.1, it can be seen from Fig. 6 that it seems that $\gamma(\kappa)$ converges to a positive number as $\kappa\to 0$. However, if the mesh is refined, then it looks like $\gamma(\kappa)$ really converges to 0 as $\kappa\to 0$.

As in the case of the 1D baker's map, the sine shear flow also enhances mixing greatly. We plot the line $\gamma=\pi^2\kappa$ in the figure and we can see that the simulated decay rates are much greater than $\kappa\pi^2$, the eigenvalue of the Laplacian operator

$$-\kappa\left(\frac{\partial^2}{\partial x^2}+\frac{\partial^2}{\partial y^2}\right).$$

Such enhancement does not contradict with the fact that the enhanced rate may still go to zero as $\kappa\to 0$. In fact, this will be proved theoretically in the next section under certain plausible conditions on the flows.

IV. ANALYTIC RESULTS

In this section, we prove analytically that the decay rate tends to zero as $\kappa\to 0$ under some reasonable conditions on the flows. We note that once we can show that $\gamma(\kappa,c^0)\to 0$ for some initial concentration c^0, then $\Gamma(\kappa)\to 0$ due to $\Gamma(\kappa)\leqslant\gamma(\kappa,c^0)$. We consider flows in both bounded and unbounded domains.

A. Flows in bounded domains

Consider the advection-diffusion equation with a source term $f(\mathbf{x},t)$ on a bounded domain S in $\mathbb{R}^n$

$$c_t+\nabla c\cdot\mathbf{v}=\kappa\Delta c+f(\mathbf{x},t),$$

$$c(\mathbf{x},t_0)=c^0(\mathbf{x}),$$

$$\left.\frac{\partial c}{\partial n}\right|_{\partial S}=0. \tag{24}$$

Here we fix the Neumann boundary condition $(\partial c/\partial n)|_{\partial S}=0$ for concreteness, but our results below are equally valid

for Dirichlet or spatially periodic boundary conditions.

In what follows, $H^n(S)$ $(n=0,1,2,\ldots)$ denotes the usual Sobolev space (see, e.g., [16]), which consists of all functions that n time differentiable in the sense of distribution and whose up to nth order derivatives are square-integrable.

We first show that the diffusive scalar converges to the conservative scalar as $\kappa \to 0$.

Theorem 4.1: *Suppose that the velocity* $\mathbf{v}$ *and the source* f *have bounded gradients over* S *and the initial condition* $c^0 \in H^1(S)$. *Then the solution* $c(\mathbf{x},t;\kappa)$ *of (26) has the following properties*:

(i) For any $T>0$ *and* $\kappa_0>0$, *the set* $\{c(\mathbf{x},t;\kappa)\,|\,0<\kappa \leqslant \kappa_0\}$ *is bounded in* $C([t_0,T];H^1(S))$.

(ii) As $\kappa \to 0$, *the solution* $c(\mathbf{x},t;\kappa)$ *converges star-weakly in* $C\{[t_0,T];H^1(S)\}$ *to the solution* $\bar{c}(\mathbf{x},t)$ *of the conservative equation*

$$\bar{c}_t + \nabla \bar{c} \cdot \mathbf{v} = f, \tag{25}$$

$$\bar{c}(\mathbf{x},t_0) = c^0(\mathbf{x}), \quad \bar{c}(\mathbf{x},T) = c_T(\mathbf{x}), \tag{26}$$

where $c_T(\mathbf{x}) = \lim_{\kappa \to 0} c(\mathbf{x},T;\kappa)$ *weakly in* $H^1(S)$ *and strongly in* $L^2(S)$.

Proof:

(i) The boundedness is the result of Proposition 2 of [12].

(ii) From (i) it follows that there exists a sequence $c_n(\mathbf{x},t)=c(\mathbf{x},t;\kappa_n)$ such that c_n converge to $\bar{c}$ star-weakly in $C\{[t_0,T];H^1(S)\}$, that is

$$\lim_{n\to\infty} \int_{t_0}^{T} \int_S \nabla c_n \nabla g dA dt = \lim_{n\to\infty} \int_{t_0}^{T} \int_S \nabla \bar{c} \nabla g dA dt \quad \text{for every } g \in L^1\{[t_0,T];H^1(S)\}.$$

Multiplying (24) by g and integrating by parts over $S \times (t_0,T)$, we obtain

$$\int_S [c_n(\mathbf{x},T)g(\mathbf{x},T) - c^0(\mathbf{x})g(\mathbf{x},t_0)]dA + \int_{t_0}^{T}\int_S (-c_n g_t + g \nabla c_n \cdot \mathbf{v}) dA dt = -\kappa_n \int_{t_0}^{T}\int_S \nabla c_n \nabla g dA dt + \int_{t_0}^{T}\int_S f g dA dt. \tag{27}$$

Since $c_n(\mathbf{x},T)$ are bounded in $H^1(S)$, there exists a subsequence, still denoted by $\{c_n(\mathbf{x},T)\}$, such that $c_n(\mathbf{x},T)$ converge to $c_T(\mathbf{x})$ weakly in $H^1(S)$ and strongly in $L^2(S)$. Taking the limit as $n\to\infty$ in the above equation gives

$$\int_S [c_T(\mathbf{x})g(\mathbf{x},T) - c^0(\mathbf{x})g(\mathbf{x},t_0)]dA - \int_{t_0}^{T}\int_S \bar{c} g_t dA dt + \int_{t_0}^{T}\int_S g \nabla \bar{c} \cdot \mathbf{v} dA dt = \int_{t_0}^{T}\int_S f g dA dt. \tag{28}$$

Taking $g(\mathbf{x},t_0)=g(\mathbf{x},T)=0$, we deduce that

$$\bar{c}_t + \nabla \bar{c} \cdot \mathbf{v} = f$$

in the sense of distribution. It then follows from (28) that

$$\int_S [c_T(\mathbf{x}) - \bar{c}(\mathbf{x},T)]g(\mathbf{x},T)dA + \int_S [\bar{c}(\mathbf{x},t_0) - c^0(\mathbf{x})]g(\mathbf{x},t_0)dA = 0. \tag{29}$$

Taking $g(\mathbf{x},T)=0$, we obtain

$$\bar{c}(\mathbf{x},t_0) = c^0(\mathbf{x}). \tag{30}$$

Taking $g(\mathbf{x},t_0)=0$, we obtain

$$\bar{c}(\mathbf{x},T) = c_T(\mathbf{x}). \tag{31}$$

This completes the proof.

To derive a reasonable condition on flows, we note that, by Proposition 2.1, there exists a positive constant $M(\kappa,c^0)$ such that

$$\|c(t,\kappa)\|_2 \leqslant M(\kappa,c^0)\|c^0\|_2 \exp\{[\kappa - \gamma(\kappa)](t-t_0)\} \tag{32}$$

for all $t \geqslant t_0$. Therefore, the constant

$$M^*(\kappa,c^0) = \sup_{t\geqslant t_0} e^{(\gamma(\kappa)-\kappa)(t-t_0)} \frac{\|c(t,\kappa)\|_2}{\|c^0\|_2} \leqslant M(\kappa,c^0) < \infty, \tag{33}$$

and (32) is still true if $M(\kappa,c^0)$ is replaced by $M^*(\kappa,c^0)$. As we discussed in Sec. II, $M^*(\kappa,c^0)$ may not be uniformly bounded as $\kappa \to 0$. If we assume that it is so, then we can show the decay rate $\gamma(\kappa,c^0) \to 0$ as $\kappa \to 0$. Therefore, the boundedness of $M^*(\kappa,c^0)$ becomes a crucial problem.

Before we prove this result, it is useful to check whether or not such assumption is reasonable. Since it is difficult to prove it analytically, we appeal to numerical results. We first look at the mixing induced by 1D baker's map with $\alpha=0.4$ and solve the mixing problem numerically as in Sec. III B. This time the initial condition is the same, but the more realistic homogeneous Neumann boundary conditions are used. The bound $M^*(\kappa,c^0)$ is approximately computed by the formula

$$M^*(\kappa,c^0,T) = \sup_{t_0\leqslant t\leqslant T} \frac{\|c(t,\kappa)\|_2}{\|c^0\|_2} \exp\{[\gamma(\kappa,c^0,T) - \kappa](t-t_0)\}, \tag{34}$$

$$\gamma(\kappa,c^0,T) = -\frac{1}{T-t_0} \ln \frac{\|c(T,\kappa)\|_2}{\|c^0\|_2}. \tag{35}$$

From Fig. 7, we can see that $M^*(\kappa,c^0,T)$ should be uniformly bounded as $\kappa \to 0$ since the values of M^* at small κ from 10^{-11} to 10^{-15} are almost the same. Also, M^* is almost constant in T after $T=20$. This shows that $T=20$ would be large enough to obtain the correct approximation of M^*.

We now look at another example

$$v_1(x,y,t) = \begin{cases} \sin(\pi x)\cos(\pi y) & \text{if } n \leqslant t < n+0.5, \\ -\sin(2\pi x)\cos(\pi y) & \text{if } n+0.5 \leqslant t < n+1, \end{cases}$$

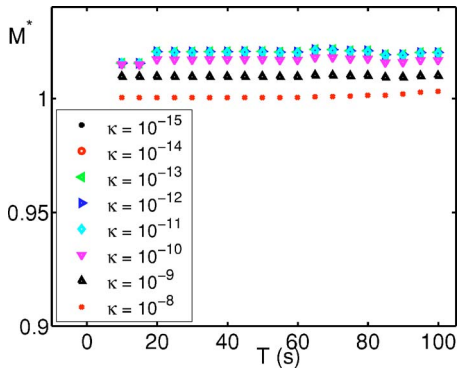

FIG. 7. (Color online) The bound $M^*(\kappa,T)$ for the 1D baker's map ($\alpha=0.4$) defined by (6), with the diffusivities $\kappa=10^{-15},\ldots,10^{-8}$ (cm^2/s). The unit of the time T is s.

$$v_2(x,y,t)=\begin{cases}-\cos(\pi x)\sin(\pi y) & \text{if } n\leqslant t<n+0.5,\\ 2\cos(2\pi x)\sin(\pi y) & \text{if } n+0.5\leqslant t<n+1.\end{cases} \tag{36}$$

Using the finite element method (with mesh size 0.05) as in Sec. III C, we solve Eq. (16) with Neumann boundary conditions and the initial concentration

$$c^0(x,y)=\begin{cases}1 & \text{if } 0\leqslant x\leqslant 1/2 \text{ and } 0\leqslant y\leqslant 1,\\ 0 & \text{if } 1/2<x\leqslant 1 \text{ and } 0\leqslant y\leqslant 1.\end{cases}$$

Figure 8 shows that the situation here is the same as in the case of the 1D baker's map and $M^*(\kappa)$ is uniformly bounded in the limit.

These numerical results could suggest that a large classes of flows have the uniform boundedness property.

Theorem 4.2: *Suppose that the velocity* $\mathbf{v}$ *has bounded gradients over* S. *If* $\mathbf{v}$ *is a velocity field such that the bound* $M^*(\kappa,c^0)$ *for some initial condition* $c^0\in H^1(S)$ *is uniformly bounded as* $\kappa\to 0$, *then the decay rate* $\gamma(\kappa,c^0)$ *of the solution* c *of* (16) *tends to zero as* $\kappa\to 0$.

Proof: We argue by contradiction. Suppose that $\gamma_0=\inf_{\kappa>0}\gamma(\kappa,c^0)>0$. By (32), we have

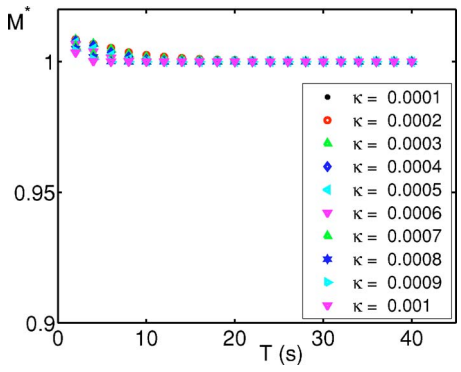

FIG. 8. (Color online) The bound $M^*(\kappa,T)$ for the flow defined by (36), with the diffusivities $\kappa=0.0001,\ldots,0.001$ (cm^2/s). The unit of the time T is s.

$$\|c(t;\kappa)\|_2\leqslant M^*(\kappa)\|c^0\|_2\exp\{[\kappa-\gamma(\kappa)](t-t_0)\}\quad \text{for all } t\geqslant t_0. \tag{37}$$

Letting $\kappa\to 0$, we deduce from part (ii) of Theorem 4.1 that

$$\|\bar{c}(t)\|_2\leqslant M_0\|c^0\|_2\exp[\gamma_0(t_0-t)]\quad \text{for all } t\geqslant t_0, \tag{38}$$

where $M_0=\sup_{0<\kappa\leqslant\kappa_0}M^*(\kappa)$ and $\kappa_0>0$. This is in contradiction with the conservation of the solution $\bar{c}$ since t can be arbitrarily large.

B. Flows in unbounded domains

For the flows in an unbounded domain $S=\mathbb{R}^n$, we seek to describe the large time and long-distance behavior of the evolution of the passive scalar governed by Eq. (1). Therefore we introduce a small parameter ϵ and the scaling of variables

$$t=\frac{s}{\epsilon^2},\quad \mathbf{x}=\frac{\mathbf{y}}{\epsilon},$$

and denote $c_\kappa^\epsilon(\mathbf{y},s)=\epsilon^{-n}c_\kappa(\mathbf{y}/\epsilon,s/\epsilon^2)$. The subscript κ indicates that c_κ is the solution of (1) corresponding to the diffusivity κ. It then follows from (1) that

$$\frac{\partial c_\kappa^\epsilon}{\partial s}+\epsilon^{-1}\mathbf{v}\left(\frac{\mathbf{y}}{\epsilon},\frac{s}{\epsilon^2}\right)\cdot\nabla c_\kappa^\epsilon=\kappa\Delta c_\kappa^\epsilon. \tag{39}$$

In this section, we assume that the velocity $\mathbf{v}$ satisfies the periodic boundary condition

$$\mathbf{v}(\mathbf{x}+Le,t)=\mathbf{v}(\mathbf{x},t),$$

$$\mathbf{v}(\mathbf{x},t+T)=\mathbf{v}(\mathbf{x},t), \tag{40}$$

where L,T are the periods and e is any integer vector. We consider the above equation on a cube Ω of side L in $\mathbb{R}^n$.

Majda and Kramer [17] derived the following homogenized effective diffusion equation of (39)

$$\frac{\partial c_\kappa^*}{\partial s}=\sum_{i,j=1}^n a_{ij}^\kappa\frac{\partial^2 c_\kappa^*}{\partial y_i\partial y_j},$$

$$c_\kappa^*(\mathbf{y},0)=c_0(\mathbf{y}), \tag{41}$$

where $\varphi_\kappa^i=\varphi_\kappa^i(\mathbf{z},\tau)$ are spatial L-periodic and time T-periodic solutions of

$$\frac{\partial\varphi_\kappa^i}{\partial\tau}+\mathbf{v}(\mathbf{z},\tau)\cdot\nabla_z\varphi_\kappa^i=\kappa\Delta_z\varphi_\kappa^i-v_i(\mathbf{z},\tau),\quad i=1,2,\ldots,n, \tag{42}$$

v_i is the ith component of $\mathbf{v}$, and

$$a_{ij}^\kappa=\kappa\delta_{ij}-\frac{1}{2Tmes(\Omega)}\int_0^T\int_\Omega[\varphi_\kappa^i v_j(\mathbf{z},\tau)+\varphi_\kappa^j v_i(\mathbf{z},\tau)]dzd\tau,$$

$$\delta_{ij}=\begin{cases}1, & i=j,\\ 0, & i\neq j.\end{cases}$$

The matrix $\mathbf{A}_\kappa=(a_{ij}^\kappa)$ is called *effective diffusivity* matrix of (1). It can be written as

$$\mathbf{A}_\kappa = \kappa \mathbf{I} + \mathbf{\Phi}_\kappa,$$

where $\mathbf{I}$ is the identity matrix and $\mathbf{\Phi}_\kappa = (\phi_\kappa^{ij})$ with

$$\phi_\kappa^{ij} = -\frac{1}{2Tmes(\Omega)} \int_0^T \int_\Omega [\varphi_\kappa^i v_j(\mathbf{z},\tau) + \varphi_\kappa^j v_i(\mathbf{z},\tau)] dz d\tau.$$

Since the matrix $\mathbf{\Phi}_\kappa$ is non-negative-definite, it is referred as convection-enhanced diffusivity matrix in [17], which represents the additional diffusivity due to the flow.

It was rigorously proved in [17]. that the rescaled scalar field $c_\kappa^\epsilon(\mathbf{y},s)$ converges to $c_\kappa^*(\mathbf{y},s)$ in the following sense:

$$\lim_{\epsilon \to 0} \sup_{t_0 \leqslant s \leqslant T} \sup_{\mathbf{y} \in \mathbb{R}^n} |c_\kappa^\epsilon(\mathbf{y},s) - c_\kappa^*(\mathbf{y},s)| = 0$$

for every finite $T > 0$, provided that $c_0(\mathbf{y})$ and $\mathbf{v}$ satisfy some mild smoothness and boundedness conditions.

Using Theorem 4.1, we want to show that the effective diffusivity matrix $\mathbf{A}_\kappa$ tends to zero as $\kappa \to 0$.

Theorem 4.3: *Suppose that the velocity* $\mathbf{v}$ *has bounded gradients over* $\mathbb{R}^n$. *Then the effective diffusivity matrix* $\mathbf{A}_\kappa$ *tends to zero as* $\kappa \to 0$.

Proof: Applying Theorem 4.1 to Eq. (42), we deduce that

$$\begin{aligned} a_{ij} &= \lim_{\kappa \to 0} a_{ij}^\kappa \\ &= \lim_{\kappa \to 0} \left(\kappa \delta_{ij} - \frac{1}{2Tmes(\Omega)} \right. \\ &\quad \left. \times \int_0^T \int_\Omega [\varphi_\kappa^i v_j(\mathbf{z},\tau) + \varphi_\kappa^j v_i(\mathbf{z},\tau)] dz d\tau \right) \\ &= -\frac{1}{2Tmes(\Omega)} \int_0^T \int_\Omega [\varphi^i v_j(\mathbf{z},\tau) + \varphi^j v_i(\mathbf{z},\tau)] dz d\tau, \end{aligned}$$

where φ^i is the solution of

$$\frac{\partial \varphi^i}{\partial \tau} + \mathbf{v}(\mathbf{z},\tau) \cdot \nabla_z \varphi^i = -v_i(\mathbf{z},\tau), \quad i = 1,2,\ldots,n.$$

Multiplying the equation by φ^j and integrating over $\Omega \times (0,T)$, we obtain

$$\int_0^T \int_\Omega [\varphi^i v_j(\mathbf{z},\tau) + \varphi^j v_i(\mathbf{z},\tau)] dz d\tau = 0.$$

Hence $a_{ij} = 0$. This completes the proof.

V. CONCLUSIONS

We have discussed the limit behavior of the decay rate of variance of a passive and diffusive scalar in a flow field as the diffusivity of the scalar goes to zero. Motivated by the concept of the fast dynamo in the dynamo theory, we have defined a flow as *fast mixer* if the decay rate remains away from zero as the diffusivity goes to zero. We repeated numerical simulations with flow maps and velocity fields used in the existing literature, including the lattice map (2) and (3) (see [1]), the 1D baker's map (6) (see [2,10]), and the sinusoidal shear flow (see, e.g., [4,11]). Our simulations showed that, in all cases, the decay rate tends to zero as $\kappa \to 0$. This result has been theoretically proved for the flows in a bounded domain if the flow is such that the constants $M^*(\kappa)$ in the following inequality are uniformly bounded as $\kappa \to 0$

$$\|c(t;\kappa)\|_2 \leqslant M^*(\kappa) \|c^0\|_2 \exp\{[\kappa - \gamma(\kappa)](t - t_0)\} \text{ for all } t \geqslant t_0.$$

For the open flows in the whole space, we showed that the effective diffusivity matrix tends to zero in the limit without the above conditions for the closed flow. In conclusion, although a fast mixer might exist, it could be very difficult to find one.

To completely solve the fast mixer problem, the study of the boundedness of $M^*(\kappa)$ becomes crucial. With the 1D baker's map and the sine-cosine shear flow we numerically showed that such boundedness is possible and then it could be plausible to guess so for most other velocity fields. But it is challenging problem to find conditions on a velocity field such that the above boundedness holds.

ACKNOWLEDGMENTS

The author thanks George Haller for suggesting this problem to him and constant discussions when he worked as a postdoctoral associate at MIT. He thanks Olivier Grunberg, Tom Peacock, Hayder Salman, and Enirque Zuazua for their valuable comments. This work was supported by the UCA start-up fund.

[1] R. T. Pierrehumbert, Chaos, Solitons Fractals **4**, 1091 (1994).
[2] D. R. Fereday, P. H. Haynes, and A. Wonhas, Phys. Rev. E **65**, 035301(R) (2002).
[3] S. Childress and A. Gilbert, *Stretch, Twist, and Fold: The Fast Dynamo* (Springer-Verlag, Berlin, 1995).
[4] T. M. Antonsen, Z. Fan, E. Ott, and E. Garcia-Lopez, Phys. Fluids **8**, 3094 (1996).
[5] V. Toussaint, P. Carriére, J. Scott, and J.-N. Gence, Phys. Fluids **12**, 2834 (2000).
[6] A. Pikovsky and O. Popovych, Europhys. Lett. **61**, 625 (2003).
[7] M. Giona, S. Cerbelli, and V. Vitacolonna, J. Fluid Mech. **513**, 221 (2004).
[8] M. Giona, V. Vitacolonna, S. Cerbelli, and A. Adrover, Phys. Rev. E **70**, 046224 (2004).
[9] A. Fannjiang and G. Papanicolaou, SIAM J. Appl. Math. **54**, 333 (1994).
[10] A. Wonhas and J. C. Vassilicos, Phys. Rev. E **66**, 051205 (2002).
[11] D. R. Fereday and P. H. Haynes, "Scalar decay in two-dimensional chaotic advection and the Batchelor-regime turbulence" (preprint).
[12] W. Liu and G. Haller, Physica D **188**, 1 (2004).
[13] R. Pierrehumbert, Chaos **10**, 61 (2000).

[14] W. F. Ames, *Numerical Methods for Partial Differential Equations*, 2nd ed. (Academic, New York, 1977).
[15] Erik G. Thompson, *Introduction to the Finite Element Method: Theory, Programming and Applications* (Wiley, Hoboken, 2005).
[16] R. Adams, *Sobolev Spaces* (Academic, New York, 1975).
[17] Andrew J. Majda and Peter R. Kramer, Phys. Rep. **314**, 237 (1999).